

Synthesis, molecular structure, mesomorphism and DFT/TD-DFT calculations of square-planar bis[1-((*p*-tolylimino)methyl)naphthalen-2-olato- κ^2 N,O]nickel and copper(II) complexes

Afsana Mim ^a, Mohammed Enamullah ^{a,*}, Imdadul Haque ^a, Abdulrahman Mohabbat ^b, Christoph Janiak ^{b,*}

^a Department of Chemistry, Jahangirnagar University, Dhaka 1342, Bangladesh

^b Institut für Anorganische Chemie und Strukturchemie, Universität Düsseldorf, Universitätsstr. 1, Düsseldorf D-40225, Germany



ARTICLE INFO

Keywords:
Ni and Cu(II) schiff base complexes
X-ray structure
Mesomorphism
Cyclic voltammograms
DFT/TD-DFT calculations

ABSTRACT

Reaction of the Schiff base ligand (E)-1-((*p*-tolylimino)methyl)naphthalen-2-ol (HL) with nickel(II) and copper (II) acetate provides the bis[1-((*p*-tolylimino)methyl)naphthalen-2-olato- κ^2 N,O]Ni and Cu(II) complexes (**1** and **2**), respectively. X-ray structure determinations reveal coordination of two N,O-chelate Schiff base ligands to the metal ion in a square-planar geometry for both the complexes. The phase purity of bulk microcrystalline samples is confirmed by Powder XRD patterns. The solid-state magnetic moment ($\mu_{\text{eff}} = 2.73$ (**1**) and $2.06 \mu_B$ (**2**)) indicates paramagnetic nature of the complexes. Thermal analyses by differential scanning calorimetry (DSC) and polarizing light microscopic (PLM) observations suggest mesomorphic property for **2**. Cyclic voltammograms recommend a quasi-reversible two one electron charge transfer processes for **2** in dimethylformamide. Geometry optimization and excited state properties by DFT/TD-DFT calculations reproduce the experimental bond distances and angles as well as the experimental electronic spectra.

1. Introduction

Transition metal-Schiff base complexes exhibiting mesomorphic properties are extensively investigated because of their unusual physicochemical properties including color, texture, magnetism, birefringence, polarizability, coordination geometry and reactivity [1–10]. Syntheses, characterizations and molecular structures of these metallomesogens (i.e., metal-containing liquid-crystalline compounds) showed continued interests and are used in optical and electrical switching, high-density optical data storage and optical computing system [4,11,12]. Of particular interest are thermotropic mesogenic properties of square-planar metal(II)-salicylaldimines and its azo-derivatives [4,10,12–14], alkyl [15–18] and alkoxy substituted compounds [8,19–21] which were investigated using differential scanning calorimetry (DSC) and polarizing light microscopic (PLM) observations. The bidentate and tetradeятate Schiff bases of salicylaldimine and its derivatives were used for the syntheses of metallomesogens mostly incorporating Cu [4,9,10,12–23], Ni [11,15–18,21,23] and VO (IV) [9,16,21,23] as a central metal ions. Indeed, some Schiff bases

compounds also showed liquid crystalline properties [3,4,9,12].

Our recent studies described the synthesis, spectroscopy, chiroptical property, stereochemistry, thermal and electrochemical analyses for a series of four-coordinated transition metal(II) complexes with *chiral*-salicylaldimines/naphthalimides having pseudotetrahedral or square-planar geometry [24–30]. X-ray molecular structures of pseudotetrahedral C_2 -symmetrical complexes explored diastereoselection and Δ vs. Λ -chirality induction at-metal upon coordination of the (R or S)-ligands and provided the two oppositely configured diastereomers of Δ -M-R and Δ -M-R (or Δ -M-S and Λ -M-S) with one being thermodynamically favoured. The diastereoselection is significantly influenced by the ligand chirality and the inter-/intra-molecular interactions in the solid state, solute-solvent interactions in solution, solvent polarity, time and temperature, metal ion selection, the crystallization process, etc. [24–30]. The Zn(II) complex with achiral (pyridyl)naphthalimides provided a racemic mixture of the two stereoisomers Δ -Zn(N,O)₂ and Λ -Zn(N,O)₂ with pseudotetrahedral C_2 -symmetry [31]. Thermal analyses of these complexes by DSC demonstrated a simple phase transformation from a crystalline solid to the molten isotropic liquid (m. p.)

* Corresponding authors.

E-mail addresses: enamullah@juniv.edu (M. Enamullah), janiak@uni-duesseldorf.de (C. Janiak).

and no mesomorphic properties were reported so far.

We reported, in continuation, the syntheses and molecular structures of (η^4 -cod)Rh(I) complexes with the achiral Schiff bases (E)-1-((Ar-imino)methyl)naphthalen-2-ol (Ar = *o*-tolyl [32] and phenyl [33]). The deprotonated Schiff base ligand coordinates to the Rh(η^4 -cod)-fragment as a six-membered N,O-chelate in a distorted square-planar geometry at the rhodium atom. The similar Schiff base with Ar = *p*-tolyl and its Mn/Zn(II) complexes with proposed octahedral geometry around the metal ion were also reported [34]. This Schiff base and its derivatives showed interesting feature along the photochemical reaction [35].

We report, herein, the syntheses, mesomorphism, molecular structures and computations of the two new square-planar nickel(II) and copper(II) (**1** and **2**) complexes with the (E)-1-((Ar-imino)methyl)naphthalen-2-ol (Ar = *p*-tolyl: HL).

2. Experimental

2.1. Materials and measurements

IR spectra were recorded on a Nicolet iS10 (Thermo Scientific) spectrometer at ambient temperature. UV-vis. spectra were obtained with a Shimadzu UV 1800 spectrophotometer in chloroform at 25(1) °C. ¹H NMR spectra were recorded on a Bruker Avance DPX 400 spectrometer in DMSO-d₆ at 20 °C. Differential scanning calorimetry (DSC) was performed on a Shimadzu DSC-60 at 30–300 °C (ca. 5 °C above the melting temperature) with a heating rate of 10 K min⁻¹. Solid-state magnetic measurements (μ_{eff}) were carried out with the magnetic susceptibility balance MSB Mk1 (Sherwood Scientific Ltd.) at 25 °C. The molar conductance (Λ_m) was measured with a Mettler Toledo Fivego (Model F3) conductivity meter in dimethylformamide (DMF) at 25 °C. Electron impact (EI) mass spectra were recorded with a Thermo-Finnigan TSQ 700 mass spectrometer. The spectra clearly show the isotopic distributions patterns for the ^{63/65}Cu containing ions. Powder X-ray diffraction (PXRD) data were collected on a GNR Explorer powder X-ray diffractometer operating in the Bragg-Brentano geometry with Cu-K α radiation ($\lambda = 1.5406 \text{ \AA}$) at 40 kV and 30 mA using a zero-background silicon sample holder. Data were collected at 25 °C with a 20 step size of 0.02 ° and an integration time of 3.0 s over an angular range of 5–45 ° (20).

2.2. Synthesis of the Schiff base ligand (HL)

2-Hydroxy-1-naphthaldehyde (1.72 g, 10.0 mmol) was dissolved in 20 mL of methanol with 3–4 drops of concentrated H₂SO₄ added into the solution, which was then stirred for ca. 10 min at room temperature. An equimolar amount of *p*-toluidine (1.07 g, 10.0 mmol) dissolved in 5 mL of methanol was added slowly into this solution. The reaction mixture was then refluxed for ca. 4–5 h. Thin-layer chromatography (TLC) was run to monitor the progress of the reaction. After ca. 40 min, a precipitate was formed upon completion of the reaction and the volume of the solution was reduced to about 50% by a rotary evaporator. The precipitate was filtered off and washed three times with methanol (2 mL each). The product was dried in open air to obtain light-yellow micro-crystals of (E)-1-((*p*-tolylimino)methyl)naphthalen-2-ol (HL).

Yield: 2.23 g (80%, based on 2-Hydroxy-1-naphthaldehyde). IR (KBr): $\nu = 3057, 3022, 2972 \text{ w (H-Ar)}, 1618 \text{ vs (C=N)} \text{ and } 1581 \text{ vs (C=C) cm}^{-1}$. UV-vis. (0.108 mM, MeOH): $\lambda_{\text{max}}/\text{nm} (\epsilon_{\text{max}}/\text{L mol}^{-1} \text{ cm}^{-1}) = 320.5 (12,444), 386 (9777) \text{ and } 445 (8768)$. ¹HNMR (400 MHz, DMSO-d₆): $\delta/\text{ppm} = 2.35$ (s, 3H, CH₃), 6.98 (d, $J_{\text{HH}} = 9.2 \text{ Hz}$, 1H, H₁₇), 7.30–7.36 (m, 3H, H_{13,14,16}), 7.52–7.56 (m, 3H, H_{2,6,7}), 7.77 (d, $J_{\text{HH}} = 8.0 \text{ Hz}$, 1H, H₈), 7.91 (d, $J_{\text{HH}} = 9.2 \text{ Hz}$, 1H, H₅), 8.44 (d, $J_{\text{HH}} = 8.4 \text{ Hz}$, 1H, H₃), 9.61 (s, 1H, CHN) and 15.90 (br, 1H, OH) (for hydrogen atom numbering see Fig. 1).

2.3. Synthesis of the complexes **1** and **2**

(E)-1-((*p*-tolylimino)methyl)naphthalen-2-ol (HL, 478 mg, 2.0 mmol), dissolved in 10 mL of methanol and 2 mL of dichloromethane, was added into 10 mL of a hot methanol solution of Ni(II) or Cu(II) acetate (249 mg or 200 mg, 1.0 mmol) and stirred for 4–5 h at room temperature. The color changed to green (for Ni) or light-brown (for Cu). After 3–4 h, green (Ni) or brown (Cu) microcrystals of bis[1-((*p*-tolylimino)methyl)naphthalen-2-olato- κ^2 N,O]Ni(II) or Cu(II) (**1** or **2**) were precipitated. The precipitate was separated by filtration, washed three times with methanol (2 mL each) and dried in ambient air for several days. Suitable crystals for X-ray measurements were grown by slow diffusion of n-hexane into concentrated solutions of the complexes in dichloromethane at room temperature after 3–4 days.

2.3.1. Bis[1-((*p*-tolylimino)methyl)naphthalen-2-olato- κ^2 N,O]Ni(II) (**1**)

Yield 0.436 g (60%). – IR (KBr, cm⁻¹): 3053, 3020, 2970, 2945 w (H-Ar), 1616, 1598 vs (C=N) and 1575 vs (C=C). Conductance: $\Lambda_m = 0.61 \text{ S m}^2 \text{ mol}^{-1}$ in DMF at 25 °C. Solid-state magnetic moment: $\mu_{\text{eff.}} = 2.73 \mu\text{B}$ at 25 °C.

2.3.2. Bis[1-((*p*-tolylimino)methyl)naphthalen-2-olato- κ^2 N,O]Cu(II), (**2**)

Yield 0.474 g (70%). – IR (KBr, cm⁻¹): 3053, 3018, 2941, 2916 w (H-Ar), 1616 vs (C=N) and 1575 vs. EI-MS: m/z (%) = 583 (3) [$\text{M} = \text{Cu(L)}_2]^+$, 322 (2) [M-HL]⁺, 260 (100) [HL-H]⁺, 244 (12) [HL-OH]⁺ and 91 (12) [C₆H₅(CH₃)-H]⁺ {M = [Cu(L)₂] = C₃₆H₂₈CuN₂O₂} and HL = C₁₈H₁₅NO}. Conductance: $\Lambda_m = 0.41 \text{ S m}^2 \text{ mol}^{-1}$ in DMF at 25 °C. Solid-state magnetic moment: $\mu_{\text{eff.}} = 2.06 \mu\text{B}$ at 25 °C.

2.4. Computational method

A thorough computational procedure was employed with Gaussian 09 [36]. The initial geometries for the computations were generated from the X-ray structures of **1** and **2**, which were optimized by DFT at the B3LYP/6–31G(d) level (Fig. S4). For the Ni(II) complex (**1**), optimizations were performed for the paramagnetic high-spin (HS) ($S = 1, m = 3$) and diamagnetic low-spin (LS) ($S = 0, m = 1$) species, respectively. Excited-state properties (UV-vis. spectra) by time-dependent density functional theory (TD-DFT) were calculated at several levels of theory using the functionals B3LYP and M06 and the basis sets 6–31G(d), SDD, SVP and TZVP, respectively. The simulated spectra are almost identical with little shifting of band maxima, and are also similar with the experimental spectra (Figs. S4a, S4b). Further, spectra for both the HS ($S = 1, m = 3$) and LS ($S = 0, m = 1$) square-planar Ni-complex (**1**) were calculated at the B3LYP/6–31G(d) level. The polarization continuum model (PCM) in chloroform and 72 excited states were considered for the calculations (Tables S2–S3). Assessments on excited state properties and molecular orbital (MO) calculations were performed at the same level of theory. The calculated spectra were produced with SpecDis (version 1.71) [37] applying the Gaussian band shape with an exponential half-width of $\sigma = 0.16 \text{ eV}$.

2.5. X-ray structure determinations

Suitable crystals were carefully selected under a polarized-light microscope, covered in protective oil and mounted on a cryo-loop. The single-crystal diffraction data were collected using a Rigaku XtalAB Synergy S four circle diffractometer with a hybrid pixel array detector and a PhotonJet X-ray source for Cu-K α radiation ($\lambda = 1.54184 \text{ \AA}$) with a multilayer mirror monochromator. Data collection was done at 100 (2.0) K using ω -scans. Data reduction and absorption correction were performed with CrysAlisPro 1.171.41.105a [38]. Structure analysis and refinement: The structures were solved by direct methods (SHELXT-2015), Full-matrix least-square refinements on F^2 were carried out using the SHELXL-2017/1 program package in OLEX 2.1.3 [39–41]. All hydrogen atoms on C were positioned geometrically (with

$C-H=0.95\text{ \AA}$ for aromatic and aliphatic CH, $C-H=0.99\text{ \AA}$ for CH_2 and $C-H=0.98\text{ \AA}$ for CH_3) and refined using riding models (AFIX 43, 23 and 137 with $U_{iso}(H)=1.2 U_{eq}(CH, CH_2)$ and $1.5 U_{eq}(CH_3)$). Crystal data and details on the structure refinement are given in Table 1. Graphics were drawn with the program DIAMOND [42]. The CCDC numbers are 2,249,766 and 2,249,767 for 1 and 2, respectively, and contain the supplementary crystallographic data reported in this paper. These data can be obtained free of charge from the Cambridge Crystallographic Data centre via www.ccdc.cam.ac.uk/data_request/cif.

3. Results and discussion

Reaction of (E)-1-((*p*-tolylimino)methyl)naphthalen-2-ol (HL) with nickel(II) and copper(II) acetate provides the square-planar bis[1-((*p*-tolylimino)methyl)naphthalen-2-olato- κ^2N,O]Ni and Cu(II) complexes (1 and 2, respectively) (Scheme 1). Vibrational spectra feature very strong bands at $1616, 1598\text{ cm}^{-1}$ for $\nu C=N$ and at 1575 cm^{-1} for $\nu C=C$ (Fig. S1). An electron impact (EI) mass spectrum shows the parent ion peak at $m/z = 583$ for complex 2 along with several ion peaks for the fragmented species (Fig. S2). The very low molar conductance values $\Lambda_m = 0.61\text{ S m}^2\text{ mol}^{-1}$ (1) and $\Lambda_m = 0.41\text{ S m}^2\text{ mol}^{-1}$ (2) indicate a non-electrolyte nature of the complexes in DMF at 25°C .

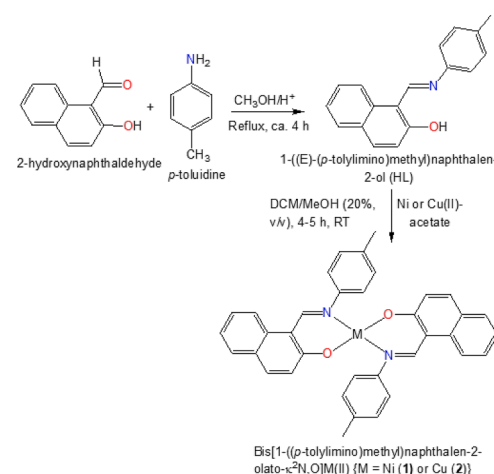
3.1. 1H NMR spectra

The 1H NMR spectrum for HL (Fig. 1) shows the signals for the methyl protons (CH_3) and the imine proton ($CH=N$) as a singlet at $\delta = 2.35$ and 9.61 ppm , respectively [32–34]. The imine proton peak is observed at relative downfield due to deshielding by the imine N atom and the benzene ring adjacent to the carbon atom. The phenolic proton gives a broad peak at $\delta = 15.90\text{ ppm}$, while the aromatic protons (Ar-H) appear as several peaks in the range of $\delta = 6.98\text{--}8.44\text{ ppm}$ (see experimental section for detailed peak assignments).

Table 1
Crystal data and structure refinement for compounds 1 and 2.

Complexes	1	2
Empirical formula	$C_{36}H_{28}N_2NiO_2$	$C_{36}H_{28}N_2CuO_2$
M (g mol $^{-1}$)	579.31	584.15
Crystal size (mm)	$0.13 \times 0.07 \times 0.06$	$0.07 \times 0.04 \times 0.04$
Temperature (K)	100(2)	100(2)
θ range ($^\circ$)	4.38 – 79.63	4.45 – 79.82
h; k; l range	$\pm 9; +10, -12; \pm 12$	$\pm 8, -9; \pm 12; +9 - 13$
Crystal system	triclinic	triclinic
Space group	P-1	P-1
a (\AA)	7.15140(10)	7.1095(4)
b (\AA)	9.7271(2)	9.9960(7)
c (\AA)	10.50320(10)	10.5004(5)
α ($^\circ$)	102.3960(10)	103.736(5)
β ($^\circ$)	96.1870(10)	99.023(5)
γ ($^\circ$)	104.7580(10)	103.832(5)
V (\AA^3)	679.768(19)	685.58(7)
Z	1	1
Dcalc (g cm $^{-3}$)	1.415	1.415
F(000)	302	303
μ (mm $^{-1}$)	1.319	1.412
Max/min transmission	1.0000 / 0.9487	1.0000 / 0.8307
Refl. measured	19,778	6629
Refl. unique	2693	2570
R_{int}	0.0334	0.0334
Parameters/restraints	188 / 0	188 / 0
Completeness	1.000	1.000
Largest diff. peak & hole ($\Delta\rho/\text{e \AA}^{-3}$)	0.448 / -0.580	1.078 / -1.269
R_1/wR_2 [$I > 2\sigma(I)$] ^a	0.0359 / 0.1303	0.0540 / 0.1583
R_1/wR_2 (all reflect.) ^a	0.0377 / 0.1326	0.0593 / 0.1619
Goodness-of-fit on F^2 ^b	1.192	1.291
CCDC number	2,249,766	2,249,767

^a $R_1 = [\sum(|F_o| - |F_c|)/\sum|F_o|]$; $wR_2 = [\sum(w(F_o^2 - F_c^2)^2)/\sum(w(F_o^2)^2)]^{1/2}$. ^b Goodness-of-fit, $S = [\sum(w(F_o^2 - F_c^2)^2)/(n - p)]^{1/2}$.



Scheme 1. Synthetic route to the formation of bis[1-((*p*-tolylimino)methyl)naphthalen-2-olato- κ^2N,O]M(II) {M = Ni (1) and Cu (2)}.

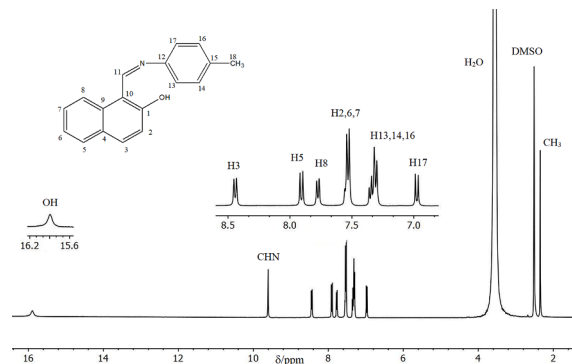


Fig. 1. 1H NMR spectrum for HL in DMSO-d₆ at 20°C .

3.2. Experimental and simulated electronic spectra (UV-vis.)

Electronic spectra for HL, 1 and 2 in chloroform (Figs. 2, 3, S4a and Table 2) feature several bands/shoulders below 500 nm due to ligand-centered $n-\pi^*/\pi-\pi^*$ transitions (LL). The spectra for the complexes further exhibit a weak broad band in the visible region (500–1000 nm) with absorption maxima (λ_{max}) at 610 (1) and 660 nm (2) due to superposition of several metal-centered d-d (MM) transitions for Ni(II) (d^8) and Cu(II) (d^9) (inset in Figs. 2, 3 and S4a) [24,28–30,43–46]. The

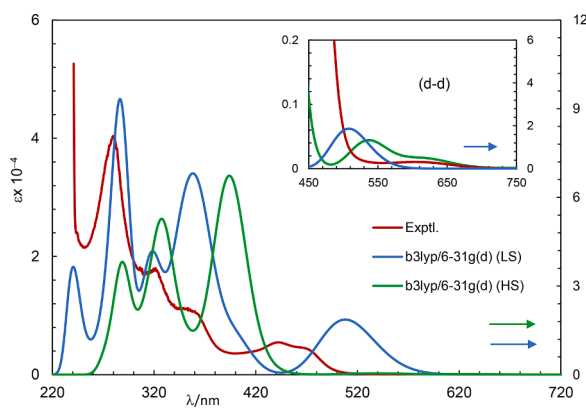


Fig. 2. Experimental spectrum for 1 (concentration ca. 0.04 mM) in chloroform at $25(1)^\circ\text{C}$. Simulated spectra for HS and LS species at B3LYP/6-31G(d) with PCM in chloroform. Spectra in the visible range are shown in the inset (Gaussian band shape with exponential half-width of $\sigma = 0.16\text{ eV}$).

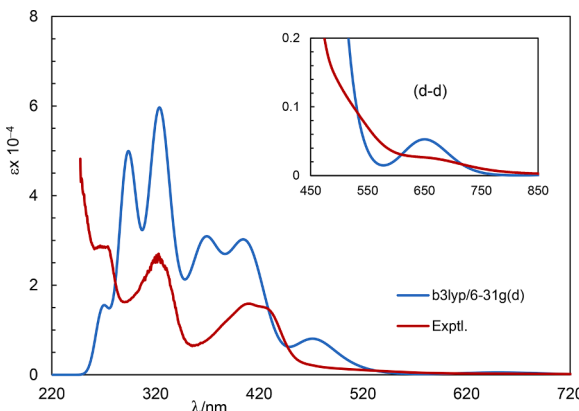


Fig. 3. Experimental spectrum for **2** (concentration ca. 0.05 mM) in chloroform at 25(1) °C. Simulated spectrum at B3LYP/6-31G(d) with PCM in chloroform. Spectra in the visible range are shown in the inset (Gaussian band shape with exponential half-width of $\sigma = 0.16$ eV).

excited state properties, that is, the UV-vis. spectra were calculated by TD-DFT for both the high-spin (HS, $S = 1, m = 3$) and low-spin (LS, $S = 0, m = 1$) square-planar Ni(II) complex (**1**) and for the Cu(II) complex (**2**) at the B3LYP/6-31G(d) level (Figs. 2 and 3). For comparison, the experimental and simulated spectra for **1** and **2** are shown in Figs. 2 and 3. The simulated spectrum for the HS Ni(II) complex shows a fair match to the experimental one, in particular, to the d-d band in the visible region at 500–700 nm (Fig. 2, inset). The simulated HS spectrum contains two weak bands with λ_{max} at 619 and 531 nm, very close to a weak broad band centered at 604 nm in the experimental spectrum (Fig. 2 and Table 2), in parallel to the analogous square-planar Ni(II)-N,O-chelate Schiff bases complexes [28]. The LS Ni(II) complex shows the simulated d-d band at 450–580 nm with $\lambda_{\text{max}} = 510$ nm. The blue shift of the d-d band for the LS complex in comparison to the HS one corresponds well to the relatively higher CFSE for the LS state (i.e., $\Delta_{\text{LS}} > \Delta_{\text{HS}}$). The HS Ni(II) complex with square-planar geometry is paramagnetic, which is confirmed by a solid-state magnetic measurement and the ^1H NMR spectrum in solution (discussed under Section 3.6). Further, the analogous pseudotetrahedral paramagnetic HS Ni(II)-N,O-chelate Schiff bases complexes [27] showed the d-d band at lower energy with $\lambda_{\text{max}} = 630$ nm (or 666 nm for the simulated spectrum), in accordance with $\Delta_{\text{Sq.}} > \Delta_{\text{Tet.}}$. These results rule out any possibility of structural change from square-planar to tetrahedral in solution and hence, suggest additional stability and integrity of the observed square-planar Ni(II) complex in the solid state (see below). For the Cu(II) complex (**2**), the experimental spectrum is very similar to the simulated spectrum (Fig. 3). The simulated spectrum shows a weak broad band in the visible region

with $\lambda_{\text{max}} = 653$ nm, very close to a broad band at 600–850 nm (with λ_{max} at ca. 660 nm) for the experimental spectrum (Fig. 3 and Table 2). Some selected and simplified assignments were made based on the molecular orbital (MOs) and population analyses for β -spin electron excitations and the data are listed in Table 2. A combined band comprised of MM and ML transitions is found at ca. 619 nm for the HOMO-4 to the LUMO+3 excitation for complex **1** (HS) and at ca. 653 nm for the HOMO-12 to LUMO excitation for complex **2**. The HOMO-4 and HOMO-12 orbitals are mainly localized at ligand moieties with a little bit of metal-d_{xy} contribution, while the LUMO+3 and LUMO orbitals are mainly localized at the metal-d_{z²} orbital with relatively little ligand contribution (Fig. 4).

3.3. X-ray crystal and optimized structures

The molecular structure determinations of **1** and **2** by single-crystal X-ray analysis disclose formation of a N₂O₂-coordination sphere around the metal ion in square-planar geometries via coordination of two N,O-chelate Schiff base ligands (Fig. 5). In contrast, the reported analogous Ni/Cu(II)-N,O-chelate Schiff base complexes showed a pseudotetrahedral geometry around the metal ion [24,27,29,30]. Both compounds **1** and **2** crystallize isostructurally in the triclinic space group P-1. One half of the molecule is present in the asymmetric unit of each crystal structure. The bond lengths and angles are listed in Table 3, comparable to the analogous Ni/Cu(II)-N,O-chelate Schiff base complexes [24,27,29,30]. A comparison of the metal-ligand bond distances in Table 3 shows that the Ni/Cu-O bond (1.831–1.888 Å) is shorter than the Ni/Cu-N bond (1.892–1.987 Å), which indicates stronger bonding interactions between the charged O[−] and M²⁺ atoms (Table 3). The imine bond (C11–N1) length (1.305–1.310 Å) is shorter than the C12–N1 bond (1.429–1.440 Å), due to a double-bond character of the former. The gas-phase optimized structures for **1** (HS- and LS-species) and **2** are shown in Fig. S5, and the calculated bond lengths and angles are comparable to the experimental results (Table 3). The gas phase optimized structure for the HS Ni(II) complex ($S = 1$) is of lower energy than the LS one ($S = 0$) by 3.85 kcal/mol. However, solid-state X-ray data (Table 3) are relatively close to the LS optimized structure due to the fact that the experimental data were collected at low temperature (100 K), where the LS state may be the ground state.

3.4. Powder X-ray diffraction

Powder X-ray diffraction (PXRD) patterns for microcrystals of **1** and **2** were measured over the 2θ range of 5–45° at 293 K (Fig. 6). The diffractograms are identical in view of the isostructural nature of **1** and **2**. A very good match of the experimental (measured at 293 K) and simulated patterns from the 100 K single crystal X-ray structures

Table 2

Selected excited state properties for **1** (HS, $S = 1$) and **2** at B3LYP/6-31G(d) level with PCM in chloroform.

Wavelength (λ/nm)	Excited states	Oscillator strength (f)	MOs contribution (%) ^a	Assignments ^b
619 (604)	5	0.0015	Compound 1 H-10→L+2 (39), H-4→L+3 (18)	MM, LM
531	8	0.0021	H-1→L+1 (22), H→L (24)	MM, LM/ML, LL
394 (475, 442)	16	0.3098	H-1→L (52), H→L (34)	MM, LM/ML, LL
329 (360, 324)	29	0.3460	H-3→L+1 (17), H-2→L+1 (62)	MM, LM, LL
290 (280)	50	0.1216	H-1→L+4 (56), H→L+4 (26)	MM, LM, LL
653 (660)	2	0.0041	Compound 2 H-12→L (48), H-11→L (14)	MM, LM
471 (430)	8	0.0758	H→L (48)	MM, LM, LL
414 (410)	11	0.1347	H→L+1 (100)	MM, LM/ML, LL
371	18	0.0713	H-1→L+2 (53)	MM, LM/ML, LL
325 (320)	27	0.3978	H-3→L+1 (46), H-2→L+1 (36)	MM, ML/LM, LL
294 (270)	45	0.2632	H→L+3 (61), H→L+4 (27)	MM, LM, LL
269	66	0.0458	H-7→L+1 (30), H→L+5 (51)	MM, LM, LL

^a β -spin electron excitations and corresponding MOs are considered.

^b H/L= HOMO/LUMO; ^b MM = metal-metal, ML/LM = metal-ligand and LL = intra-ligand transitions.

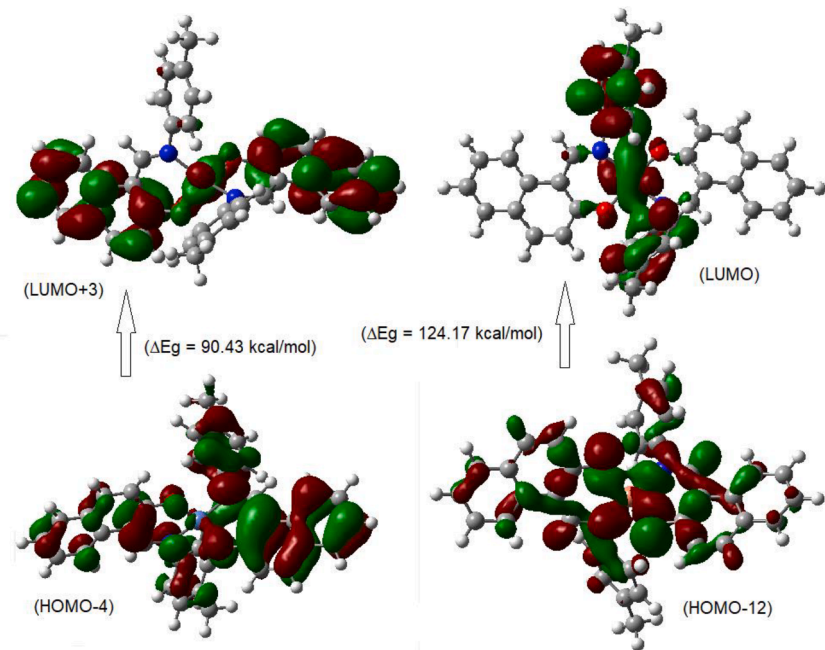


Fig. 4. HOMO-4/LUMO+3 for **1** (HS) (left) and HOMO-12/LUMO for **2** (right) for β -spin electron transitions.

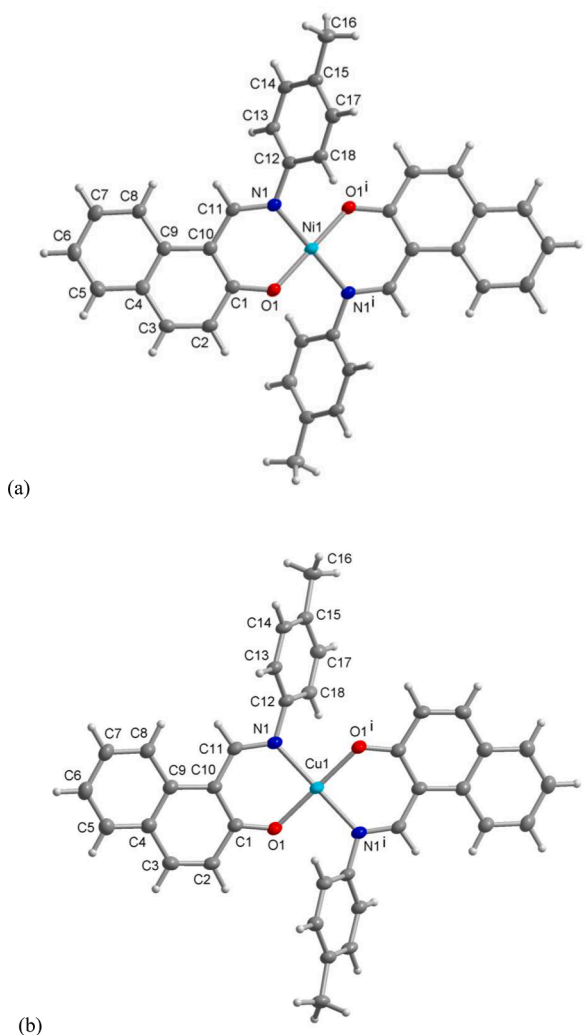


Fig. 5. Molecular structures in the crystal of **1** (a) and **2** (b). Symmetry label $i = 1-x, 1-y, -z$ in **1**, $i = 1-x, 1-y, 2-z$ in **2**.

confirms the phase purity of the bulk microcrystalline samples [27,29, 43,44]. A slight peak shift to higher 2θ angles in the simulated diffractograms is due to the lower temperature in the underlying crystal structure data with a concurrent contraction of the bond lengths and unit cell parameters.

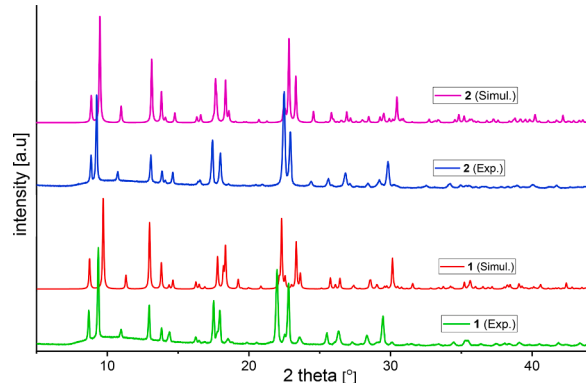
3.5. Thermal analysis and mesomorphic property

Thermal analyses for HL, **1** and **2** were carried out by differential scanning calorimetry (DSC) following the phase transformation temperature and enthalpy changes (ΔH) [24–29]. The DSC heating curve for HL shows an endothermic peak at ca. 138°C ($\Delta H = -25.4 \text{ kJ mol}^{-1}$), which corresponds to a transformation from crystalline-solid (Cr) to isotropic-liquid phase (I or m.p., Cr \rightleftharpoons I) (Fig. 7a and Table 4). The cooling curve shows no corresponding peak in the reverse direction, suggesting an irreversible phase transformation. The heating curve for the Ni(II) complex (**1**) exhibits an endothermic peak at ca. 286°C ($\Delta H = -47.3 \text{ kJ mol}^{-1}$) for a crystalline-solid (Cr) to isotropic-liquid phase (Cr \rightleftharpoons I) (Fig. 7b and Table 4). The cooling curve features an exothermic peak in the reverse direction at ca. 204°C ($\Delta H = +35.3 \text{ kJ mol}^{-1}$) for an isotropic-liquid to solid-crystal phase transformation (I \rightleftharpoons SCr), i.e., solidification of the isotropic-liquid, corresponding to a reversible phase transformation. The repeated heating curve in the second cycle for the same probe of HL and **1** reproduce similar results, suggesting their thermal stability and integrity (Fig. 7a,b and Table 4). For the Cu(II) complex (**2**), the heating curve displays two endothermic peaks at ca. 216°C ($\Delta H = -31.2 \text{ (kJ mol}^{-1})$) and 224°C ($\Delta H = -0.9 \text{ kJ mol}^{-1}$) for phase transformations from crystalline-solid to liquid-crystals (Cr \rightleftharpoons Lc) and to isotropic-liquid (Lc \rightleftharpoons I), respectively (Fig. 7c and Table 4). The cooling curve shows two exothermic peaks at ca. 175 and 166°C ($\Delta H = +4.7 \text{ kJ mol}^{-1}$) for I \rightleftharpoons Lc and Lc \rightleftharpoons SCr phase transformations, respectively. The repeated heating curve in the second cycle for the same probe gives a single endothermic peak at ca. 223°C ($\Delta H = -28.3 \text{ kJ mol}^{-1}$), which corresponds to a single-phase transformation from crystalline-solid to isotropic-liquid (Cr \rightleftharpoons I) with no liquid-crystalline phase. However, the cooling curve reproduces similar results as in the first cooling cycle (Fig. 7c and Table 4).

The mesomorphic property for **1** and **2** was examined by polarizing light microscopic (PLM) observations using a heating-cooling stage [4, 10,12–23]. The optical texture for the Cu(II) complex (**2**) during the first

Table 3Selected bond lengths (\AA) and angles ($^\circ$) in **1** and **2**.

Bond lengths (\AA) and angles ($^\circ$)	X-ray structure for 1 (M = Ni)	Optimized structures for 1 ^a		X-ray structure for 2 (M = Cu)	Optimized structure for 2 ^a
		LS (S = 0)	HS (S = 1)		
M-O1/O1 ⁱ	1.831	1.8213	1.8954/1.8925	1.888	1.8907/1.8879
M-N1/N1 ⁱ	1.892	1.8953	1.9621/1.9630	1.987	1.9582/1.9685
C1-O1/O1 ⁱ	1.302(2)	1.2962	1.2964/1.2929	1.293(3)	1.2957/1.2928
C12-N1/N1 ⁱ	1.440(2)	1.4334	1.4208/1.4234	1.429(4)	1.4232/1.4274
C11-N1/N1 ⁱ	1.310(2)	1.3133	1.3135/1.3160	1.305(4)	1.3126/1.3136
O1-M-N1/O1 ⁱ -M-N1 ⁱ	92.20	91.50	92.10/92.27	90.38	93.05/92.98
O1-M-O1 ⁱ /N1-M-N1 ⁱ	180.00	180.0	120.62/142.16	180.00	141.84/146.89
O1 ⁱ -M-N1/O1-M-N1 ⁱ	87.80	88.50	104.52/108.30	89.62	95.10/100.16

^a Optimized structure at B3LYP/6-31G(d).**Fig. 6.** Experimental (at 293 K) and simulated (from 100 K X-ray data set) PXRD patterns for **1** and **2**.

heating cycle showed a crystalline solid phase (Cr) at 40–210 °C (Fig. 8a), which subsequently melted at 212–217 °C (Fig. 8b). A liquid-crystalline phase (Lc) was observed on further heating at 219–222 °C (Fig. 8c), followed by a phase transformation to isotropic-liquid (I or m. p.) at 223–225 °C (Fig. 8d). On cooling, the isotropic-liquid (I) transformed to liquid-crystals (Lc) phase at 180–175 °C (Fig. 8e) and then to a solid crystal phase (SCr, i.e., solidification of liquid-crystals) at 160–165 °C (Fig. 8f). These results of optical observations are in parallel to the thermal (DSC) analysis (Fig. 7c and Table 4) and strongly suggest a mesomorphic property (liquid-crystals) for the Cu(II) complex (2). Optical observations for the Ni(II) complex (1) during the first heating cycle displayed a crystalline solid phase (Cr) in the range of 40–210 °C (Fig. S6a), which subsequently melted to an isotropic-liquid (I or m. p.) at 286–290 °C (Fig. S6b). The cooling cycle showed a solid crystal phase (SCr, i.e., solidification of the isotropic-liquid) at 200–205 °C (Fig. S6c). Thus, the thermal analysis and optical observations displayed no mesomorphic properties for complex 1.

3.6. Paramagnetism of the complexes

The solid-state magnetic moments $\mu_{\text{eff.}} = 2.73 \mu_B$ for **1** and $2.06 \mu_B$ for **2** at 25 °C (without diamagnetic corrections) indicate a paramagnetic nature of the complexes [43,45,47–49]. The difference to the theoretical spin-only magnetic moment for Ni (total spin $S = 1$, $\mu_{\text{eff.}} = 2.83 \mu_B$) and Cu ($S = 1/2$, $\mu_{\text{eff.}} = 1.73 \mu_B$) is due to contributions from the orbital angular magnetic momentum and/or diamagnetic contributions from the ligands [50,51]. The square-planar Ni(II) complex may have paramagnetic high-spin ($S = 1$) or a diamagnetic low-spin ($S = 0$) configuration depending on the metal-ligand interactions [28,43,52]. To check this, we measured a ^1H NMR spectrum for **1** in CDCl_3 (Fig. S3a), which shows peak broadening and shifting effects, in parallel to the paramagnetic nature of the Ni(II)-Schiff base complexes [28,43], alike the

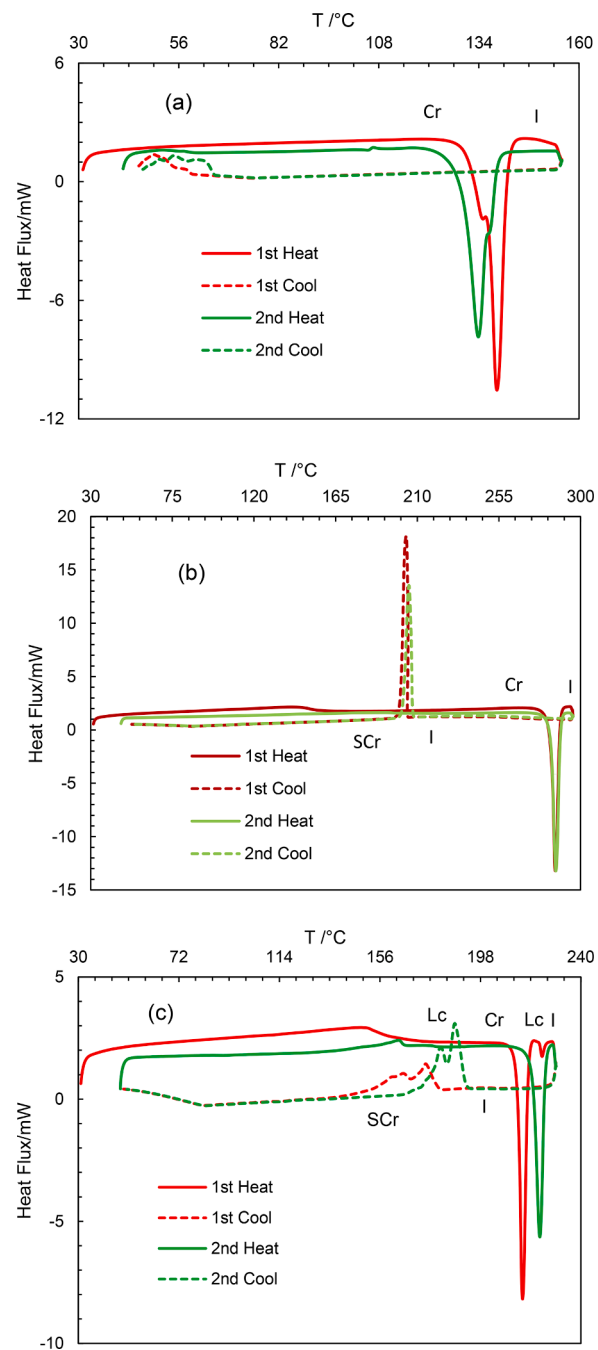
**Fig. 7.** Differential scanning calorimetry (DSC) curves for HL (a), **1** (b) and **2** (c).

Table 4Phase transformation temperatures and enthalpy changes for HL, **1** and **2**.

Compounds	Peak temperature (°C)/ΔH (kJ mol ⁻¹) [*] (1st cycle)	Peak temperature (°C)/ΔH (kJ mol ⁻¹) [*] (2nd cycle)
HL	ca. 139/-25.4 (Cr ⇌ I) (heat) No peak (cool)	ca. 134/-24.1 (Cr ⇌ I) (heat) No peak (cool)
1	ca. 286/-47.3 (Cr ⇌ I) (heat) ca. 204/+35.3 (I ⇌ S _{Cr}) (cool)	ca. 286/-45.3 (Cr ⇌ I) (heat) ca. 205/+34.3 (I ⇌ S _{Cr}) (cool)
2	ca. 216/-31.2 (Cr ⇌ Lc), 224/-0.9 (Lc ⇌ I) (heat) ca. 175 (I ⇌ Lc), 166/+4.7 (Lc ⇌ S _{Cr}) (cool)	ca. 223/-28.3 (Cr ⇌ I) (heat) ca. 187 (I ⇌ Lc), 181 (Lc ⇌ S _{Cr})/+7.5 (cool)

^{*} ΔH = Enthalpy changes.

paramagnetic spectrum for the Cu(II) complex (**2**) (Fig. S3b). These results are in good accord to the solid-state magnetic moments, and a preferred HS optimized structure for the simulated UV-vis. absorption spectra (see above).

3.7. Cyclic voltammetry

Cyclic voltammograms for **2** were recorded from -1.20 to 1.00 V versus Ag/AgCl at varying scan rates in N,N-dimethylformamide (DMF) at 25 °C (Fig. 9). The reductive scan shows two cathodic peaks at ca. -0.62 V ($I_{c1} = +7.22 \mu\text{A}$) and -1.02 V ($I_{c2} = +7.21 \mu\text{A}$), corresponding to two one electron charge transfer processes of the $[\text{CuL}_2]/[\text{CuL}_2]^-$ and $[\text{CuL}_2]^-/[\text{CuL}_2]^{2-}$ couples (L = deprotonated Schiff base ligand), respectively at a scan rate of 0.10 V s⁻¹. The oxidative scan shows corresponding anodic peaks at ca. -0.27 V ($I_{a2} = -0.31 \mu\text{A}$) and +0.67 V ($I_{a1} = -2.88 \mu\text{A}$) for $[\text{CuL}_2]^{2-}/[\text{CuL}_2]^-$ and $[\text{CuL}_2]^-/[\text{CuL}_2]$ couples, respectively [44,45,53,54]. The anodic peak at ca. -0.27 V is very weak due to the instability and/or rapid chemical transformation of the $[\text{CuL}_2]^- (\text{Cu}^+)$ species. Analyses of voltammograms at varying scan rates resulted in both the cathodic and anodic peaks becoming increasingly populated and a shift of the peaks to lower and higher potential, respectively (Fig. 9). The plot of peak current versus square root of the scan rate (i.e., I_c or I_a or I_a/I_c vs. $\nu^{1/2}$) exposed an increase of cathodic peak current (I_c) or a decrease of anodic peak current (I_a) at a constant ratio of I_a/I_c with faster scan rates (Fig. 9, inset). The straight line

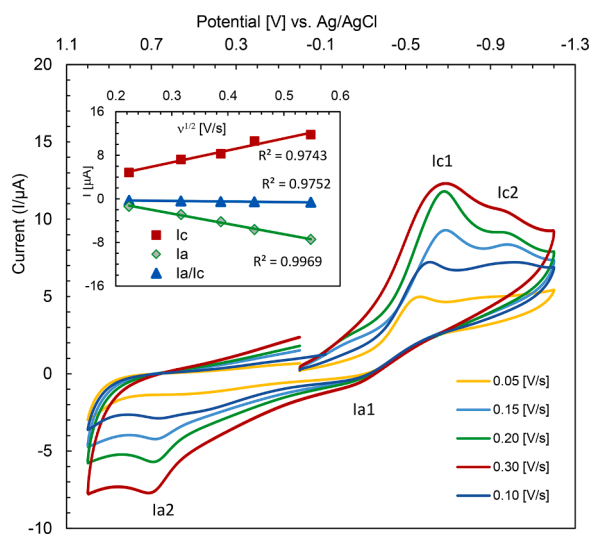


Fig. 9. Cyclic voltammograms for **2** (concentration ca. 0.5 mM) at different scan rates (ν/Vs^{-1}) using tetra-N-butyl-ammonium hexafluorophosphate (TBAP) as supporting electrolyte (concentration ca. 0.1 mM) in DMF at 25 °C (inset: plot of I_c or I_a or I_a/I_c vs. $\nu^{1/2}$).

indicates a diffusion-controlled electrochemical process in solution. The overall results suggest a quasi-reversible two one electron charge transfer processes as reported for the analogous Cu(II)-N,O-chelate Schiff base complexes [44,45,53,54].

4. Conclusions

The bis[1-((*p*-tolylimino)methyl)naphthalen-2-olato- $\kappa^2\text{N},\text{O}]$ Ni and Cu(II) (**1** and **2**) complexes were synthesized from the Schiff base ligand (E)-1-((*p*-tolylimino)methyl)naphthalen-2-ol. Molecular structures determinations reveal a coordination of two molecules of the naphthaliminato ligands to the metal(II) ions, having both complexes a square-planar geometry. Powder XRD patterns support the phase purity of the bulk microcrystalline samples. Both complexes are paramagnetic in nature. While this could be expected for the Cu(II) complex, it is unexpected for the square-planar Ni(II) complex and this observation will be the subject of further investigations. Thermal analysis by DSC and polarized light microscopic observations reveal a mesogenic property for **2**. Cyclic voltammograms demonstrate a quasi-reversible two one electron charge transfer processes for **2** in dimethylformamide. DFT/TD-DFT calculations support the experimental results of UV-vis. spectra and molecular structures. In subsequent studies we will now address the analogous metal(II) complexes in view of mesomorphism and molecular structures.

CRediT authorship contribution statement

Afsana Mim: Formal analysis, Investigation, Data curation, Writing – original draft. **Mohammed Enamullah:** Conceptualization,

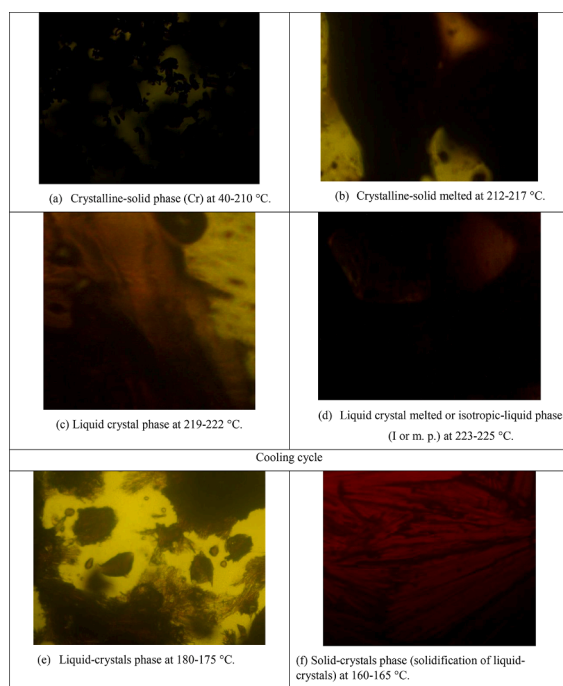


Fig. 8. Optical texture observations through polarizing light microscope (PLM) during the first heating and cooling cycle for **2**.

Methodology, Validation, Formal analysis, Investigation, Resources, Data curation, Writing – original draft, Writing – review & editing, Visualization, Supervision, Project administration, Funding acquisition. **Imdadul Haque:** Investigation, Data curation, Writing – original draft. **Abdulrahman Mohabbat:** Formal analysis, Investigation, Data curation, Writing – original draft. **Christoph Janiak:** Conceptualization, Validation, Resources, Writing – review & editing, Visualization, Project administration, Funding acquisition, Writing – original draft.

Declaration of Competing Interest

The authors declare that they have no known competing financial interests or personal relationships that could have appeared to influence the work reported in this paper.

Data availability

No data was used for the research described in the article.

Acknowledgments

The authors acknowledge the financial support from the Alexander von Humboldt Foundation (AvH), Bonn, Germany under the Research Group Linkage Program. We Thank to Professor Mominul Islam, Department of Chemistry, University of Dhaka, Bangladesh for CV measurements. For computational resource, we thank Professor ABP Lever, Department of Chemistry, York University, Toronto and the computecanada.ca (<https://ccdb.computecanada.ca>) Ontario, Canada. The research was funded by the Deutsche Forschungsgemeinschaft (DFG, German Research Foundation) under grant 440366605 (for the Rigaku diffractometer).

Supplementary materials

Supplementary material associated with this article can be found, in the online version, at doi:[10.1016/j.molstruc.2023.135669](https://doi.org/10.1016/j.molstruc.2023.135669).

References

- [1] S.A. Hudson, P.M. Maitlis, Calamitic metallomesogens: metal-containing liquid crystals with rodelike shapes, *Chem. Rev.* 93 (1993) 861–885.
- [2] P. Espinet, M.A. Esteruelas, L.A. Oro, E. Sola, Transition metal liquid crystals: advanced materials within the reach of the coordination chemist, *Coord. Chem. Rev.* 117 (1992) 215–274.
- [3] A.M. Giroud, P.M. Maitlis, Metallomesogens: metal complexes in organized fluid phases, *Angew. Chem. Int. Ed.* 30 (1991) 375–402.
- [4] R. Paschke, S. Liebsch, C. Tschierske, M.A. Oakley, E. Sinn, Synthesis and mesogenic properties of binuclear copper(II) complexes derived from salicylaldimine Schiff bases, *Inorg. Chem.* 42 (25) (2003) 8230–8240.
- [5] R. Ziessl, Schiff-based bipyridine ligands. Unusual coordination features and mesomorphic behaviour, *Coord. Chem. Rev.* 216–217 (2001) 195–223.
- [6] N. Hoshino, Liquid crystal properties of metal-salicylaldimine complexes: chemical modifications towards lower symmetry, *Coord. Chem. Rev.* 174 (1998) 77–108.
- [7] D.W. Bruce, Dalton perspectives. the synthesis and properties of metal-containing liquid-crystal systems: what can the metal do for you? *J. Chem. Soc. Dalton Trans.* (1993) 2983–2989.
- [8] R.W. Date, E.F. Iglesias, K.E. Rowe, J.M. Elliott, D.W. Bruce, Metallomesogens by ligand design, *Dalton Trans.* (2003) 1914–1931.
- [9] M. Cano, L. Oriol, M. Pinol, J.L. Serrano, Photopolymerization of reactive mesogenic Schiff bases and related metallomesogens, *Chem. Mater.* 11 (1) (1999) 94–100.
- [10] B. Borchers, W. Haase, Investigations on the liquid crystalline phase of Schiff's base complexes of copper(II) and their corresponding ligands, *Mol. Cryst. Liq. Cryst.* 209 (1991) 319–328.
- [11] I. Aiello, M. Ghedini, M.L. Deda, D. Pucci, O. Francescangeli, Synthesis, mesomorphism, and spectroscopic characterization of bis[4-(*n*-alkoxy)-5-(*p*-tetradecylphenylazo)]-substituted (N,N'-salicylidenediaminato)nickel(II) complexes, *Eur. J. Inorg. Chem.* (1999) 1367–1372.
- [12] Y. Tian, F. Su, P. Xing, Y. Zhao, X. Tang, X. Zhao, E. Zhou, Synthesis of a new series of chiral Schiff's bases and their copper complexes, *Liq. Cryst.* 20 (1996) 139–145.
- [13] Z. Rezvani, B. Divband, A.R. Abbasi, K. Nejati, Liquid crystalline properties of copper(II) complexes derived from azo-containing salicylaldimine ligand, *Polyhedron* 25 (9) (2006) 1915–1920.
- [14] C. Crete, L. Cseh, B.J. Tang, V. Sasca, V. Badea, E.I. Szerb, G. Mehl, S. Shova, O. Costisor, Mononuclear Cu(II) complexes of novel salicylidene Schiff bases: synthesis and mesogenic properties, *Liquid Cryst.* 42 (2015) 1139–1147.
- [15] R. Paschke, D. Balkow, U. Baumeister, H. Hartung, J.R. Chipperfield, A.B. Blake, P. G. Nelson, G.W. Gray, Di(5-substituted-salicylidene)ethylene diaminato-complexes (Part II). Mesomorphic properties of di(5-alkylsalicylidene)ethylene diaminato nickel(II) and copper(II) complexes and an X-ray structure determination of di(5-hexyloxy salicylidene)ethylenediaminato nickel(II), *Mol. Cryst. Liq. Cryst.* 188 (1990) 105–118.
- [16] A.B. Blake, J.R. Chipperfield, W. Hussain, R. Paschke, E. Sinn, Effects of ligand substituents (F for H; OR for R) on mesogenic properties of M(Salen) derivatives (M = Cu, Ni, VO). New fluoro-substituted complexes and crystal structure of the mesogen Ni(5-hexylSalen), *Inorg. Chem.* 34 (1995) 1125–1129.
- [17] T.D. Shaffer, K.A. Shet, Mesomorphic transition metal N₂O₂ chelates, *Mol. Cryst. Liq. Cryst.* 172 (1989) 27–39.
- [18] Z. Rezvani, L.R. Ahar, K. Nejati, S.M. Seyedahmadian, Syntheses, characterization and liquid crystalline properties of new bis[5-((4-N-alkoxyphenylazo)-N-(N-alkyl)-salicylaldiminato]copper(II) and nickel(II) complex homologues, *Acta Chim. Slov.* 51 (2004) 675–686.
- [19] N. Hoshino, H. Murakami, Y. Matsunaga, T. Inabe, Y. Maruyama, Liquid crystalline copper(II) complexes of N-salicylideneaniline derivatives. Mesomorphic properties and a crystal structure, *Inorg. Chem.* 29 (1990) 1177–1181.
- [20] A.A. Khandar, Z. Rezvani, Preparation and thermal properties of the bis[5-((4-heptyloxyphenylazo)-N-(4-alkoxyphenyl)-salicylaldiminato]copper(II) complex homologues, *Polyhedron* 18 (1998) 129–133.
- [21] K. Nejati, Z. Rezvani, Syntheses, characterization and mesomorphic properties of new bis(alkoxyphenylazo)-substituted N,N'-salicylidene diiminato Ni(II), Cu(II) and VO(IV) complexes, *New J. Chem.* 27 (2003) 1665–1669.
- [22] B. Bilgin-Eran, Ç. Yörür, S. Uzman, Synthesis and mesomorphic properties of new imines and copper(II) complexes, *J. Organomet. Chem.* 655 (2002) 105–110.
- [23] J. Barbera, A.M. Levelut, M. Marcos, P. Romero, J.L. Serrano, X-ray diffraction study of some mesogenic copper, nickel and vanadyl complexes, *Liq. Cryst.* 10 (1991) 119–126.
- [24] M. Enamullah, A.K.M.R. Uddin, G. Pescitelli, R. Berardozzi, G. Makhlofui, V. Vasyleva, A.C. Chamayou, C. Janiak, Induced chirality-at-metal and diastereoselectivity at Δ/Λ-configured distorted square-planar copper complexes by enantiopure Schiff base ligands: combined circular dichroism, DFT and X-ray structural studies, *Dalton Trans.* 43 (2014) 3313–3329.
- [25] M. Górecki, M. Enamullah, M.A. Islam, M.K. Islam, S.P. Höfert, D. Woschko, C. Janiak, G. Pescitelli, Synthesis and characterization of bis[(R or S)-N-1-(X-C₆H₄)ethyl-2-oxo-1-naphthaldiminato-κ²N,O]Δ/Λ-cobalt(II) (X = H, p-CH₃O, p-Br) with symmetry- and distance-dependent vibrational circular dichroism enhancement and sign inversion, *Inorg. Chem.* 60 (2021) 14116–14131.
- [26] M. Enamullah, G. Makhlofui, R. Ahmed, B.A. Joy, M.A. Islam, D. Padula, H. Hunter, G. Pescitelli, C. Janiak, Synthesis, X-ray and spectroscopic study of dissymmetric tetrahedral zinc(II) complexes from chiral Schiff base naphthaldiminate ligands with apparent exception to the ECD exciton chirality, *Inorg. Chem.* 55 (2016) 6449–6464.
- [27] A. Saadati, H.A. Rudbari, M. Aryaeifar, O. Blacque, I. Correia, M.K. Islam, D. Woschko, T.H.H. Sohi, C. Janiak, M. Enamullah, Experimental and computational studies on pseudotetrahedral nickel(II)-(R or S)-dihalogen-salicylaldimimates with Δ- or Λ-chirality induction at-metal, *CrystEngComm* 25 (2023) 365–377.
- [28] M. Enamullah, M.A. Quddus, M.R. Hasan, G. Pescitelli, R. Berardozzi, G. Makhlofui, V. Vasyleva, C. Janiak, Chirality at metal and helical ligand folding in optical isomers of chiral bis(naphthaldiminato)nickel(II) complexes, *Dalton Trans.* 45 (2016) 667–680.
- [29] N. Kordestani, H.A. Rudbari, G. Bruno, S. Rosario, J.D. Braun, D.E. Herbert, O. Blacque, I. Correia, M. Al-M. Zaman, M. Mamun Bindu, C. Janiak, M. Enamullah, Solid-state to solution helicity inversion of pseudotetrahedral chiral copper(II) complexes with 2,4-dihalo-salicylaldiminate ligands, *Dalton Trans.* 49 (2020) 8247–8264.
- [30] A.C. Chamayou, G. Makhlofui, L.A. Nafie, C. Janiak, S. Lüdeke, Solvation-induced helicity inversion of pseudotetrahedral chiral copper(II) complexes, *Inorg. Chem.* 54 (2015) 2193–2203.
- [31] M. Enamullah, M.A. Islam, B.A. Joy, B. Dittrich, G. Reiss, C. Janiak, π-π interaction leading to an inversion-symmetric complex pair of Λ- and Δ-bis[N-2-(R-pyridyl)-2-oxo-1-naphthaldiminato-κ²N,O]zinc(II), *Inorg. Chim. Acta* 482 (2018) 935–942.
- [32] C. Janiak, A.C. Chamayou, A.K.M. Royhan Uddin, M. Uddin, K.S. Hagen, M. Enamullah, Polymorphs, enantiomorphs, chirality and helicity in [Rh{N,O}(η⁴-cod)] complexes with {N,O} = salicylaldiminate Schiff base or aminocarboxylato ligands, *Dalton Trans.* 19 (2009) 3698–3709.
- [33] M. Enamullah, M.A. Islam, C. Janiak, Rh{N,O}(η⁴-cod) or (PPh₃)₂-Schiff base complexes with a Z' = 2 structure: syntheses, spectroscopy, thermalanalyses and DFT/TDDFT, *J. Mol. Struct.* 1122 (2016) 331–340.
- [34] V. Gomathi, R. Selvameena, R. Subbalakshmi, G. Valarmathy, Synthesis, spectral characterization and antimicrobial screening of Mn(II) and Zn(II) complexes derived from (E)-1-(*p*-tolylimino)methyl)naphthalene-2-ol, *Orient. J. Chem.* 29 (2) (2013) 533–538.
- [35] P.P. Levin, A.S. Tatikolov, N.L. Zaichenko, A.I. Shienok, L.S. Koltssova, I. M. Sherbakova, I.R. Mardaleishvili, A.A. Berlin, Kinetics of photochemical reactions of biphotochromic compounds based on spironaphthopyran and enamine – conjugation effect, *Photochem. Photobiol. Sci.* 15 (2016) 382–388.
- [36] M.J. Frisch, G.W. Trucks, H.B. Schlegel, G.E. Scuseria, M.A. Robb, J.R. Cheeseman, G. Scalmani, V. Barone, G.A. Petersson, H. Nakatsuji, X. Li, M. Caricato, A. V. Marenich, J. Bloino, B.G. Janesko, R. Gomperts, B. Mennucci, H.P. Hratchian, J.

- V. Ortiz, A.F. Izmaylov, J.L. Sonnemberg, D. Williams-Young, F. Ding, F. Lipparini, F. Egidi, J. Goings, B. Peng, A. Petrone, T. Henderson, D. Ranasinghe, V. G. Zakrzewski, J. Gao, N. Rega, G. Zheng, W. Liang, M. Hada, M. Ehara, K. Toyota, R. Fukuda, J. Hasegawa, M. Ishida, T. Nakajima, Y. Honda, O. Kitao, H. Nakai, T. Vreven, K. Throssell, J.J.A. Montgomery, J.E. Peralta, F. Ogliaro, M. Bearpark, J. J. Heyd, E. Brothers, K.N. Kudin, V.N. Staroverov, T.A. Keith, R. Kobayashi, J. Normand, K. Raghavachari, A. Rentell, J.C. Burant, S.S. Iyengar, J. Tomasi, M. Cossi, J.M. Illam, M. Klene, C. Adamo, R. Cammi, J.W. Ochterski, R.L. Martin, K. Morokuma, O. Farkas, J.B. Foresman, D.J. Fox, Gaussian 16, Revision A.03, Gaussian, Inc., Wallingford CT, 2016. GaussView 5.0, Wallingford, U.S.A.
- [37] T. Bruhn, A. Schaumlöffel, Y. Hemberger, G. Pescitelli, SpecDis Version 1.71, Berlin, Germany, 2017; <https://specdis-software.jimdo.com>.
- [38] CrysAlisPro, Rigaku Oxford Diffraction, release 1.171.40.103a. 2021; <http://www.rigaku.com/products/crystallography/crysalis>.
- [39] G.M. Sheldrick, Crystal structure refinement with SHELXL, *Acta Crystallogr. Sect. C Cryst. Struct. Commun.* C71 (2015) 3.
- [40] G.M. Sheldrick, A short history of SHELX, *Acta Crystallogr. A Found Crystallogr.* 64 (2008) 112.
- [41] O.V. Dolomanov, L.J. Bourhis, R.J. Gildea, J.A.K. Howard, H. Puschmann, OLEX2: a complete structure solution, refinement and analysis program, *J. Appl. Crystallogr.* 42 (2009) 339–341.
- [42] K. Brandenburg, Diamond (Version 4.5), Crystal and Molecular Structure Visualization, Crystal Impact, K. Brandenburg & H. Putz Gbr, Bonn, Germany, 2009.
- [43] I. Haque, M.S. Abdullah, M.K. Islam, M. Enamullah, Synthesis, PXRD structure, spectroscopy, cyclic voltammogram, thermal analysis and DFT/TD-DFT calculations of bis[salicylaldehydato- κ O,O']nickel(II), *Inorg. Chim. Acta* 550 (2023), 121430.
- [44] M. Enamullah, M.A. Hossain, M.K. Islam, D. Woschko, C. Janiak, Pseudotetrahedral copper(II)-complexes with enantiopure (*R*- or *S*)-2 (((aryl) ethylimino)ethyl)phenolate Schiff base ligands, *Dalton Trans.* 50 (2021) 9236–9249.
- [45] M. Enamullah, M.A. Islam, B.A. Joy, G.J. Reiß, Bis[N-2-(*R*-pyridyl)-2-oxo-1-naphthaliminato- κ^2 N,O]copper(II) (*R* = H, 4/6-CH₃): combined studies on syntheses, spectroscopy, cyclic voltammetry, thermal analyses, crystal structure and DFT/TDDFT, *Inorg. Chim. Acta* 453 (2016) 202–209.
- [46] H. Kargar, R.B. Ardakanli, V. Torabi, M. Kashani, Z. Chavoshpour-Natanzi, Z. Kazemi, V. Mirkhani, A. Sahraei, M.N. Tahir, M. Ashfaq, K.S. Munawar, Synthesis, characterization, crystal structures, DFT, TD-DFT, molecular docking and DNA binding studies of novel copper(II) and zinc(II) complexes bearing halogenated bidentate N,O-donor Schiff base ligands, *Polyhedron* 195 (2021), 114988.
- [47] T. Akitsu, Y. Einaga, Synthesis, crystal structures and electronic properties of Schiff base nickel(II) complexes: towards solvatochromism induced by a photochromic solute, *Polyhedron* 24 (2005) 1869–1877.
- [48] L.H. Abdel-Rahman, N.M. Ismail, M. Ismael, A.M. Abu-Dief, E.A.-H. Ahmed, Synthesis, characterization, DFT calculations and biological studies of Mn(II), Fe (II), Co(II) and Cd(II) complexes based on a tetradentate ONNO donor Schiff base ligand, *J. Mol. Struct.* 1134 (2017) 851–862.
- [49] S.M. Abdallah, G.G. Mohamed, M.A. Zayed, M.S.A. El-Ela, Spectroscopic study of molecular structures of novel Schiff base derived from *o*-phthaldehyde and 2-aminophenol and its coordination compounds together with their biological activity, *Spectrochim. Acta Part A* 73 (2009) 833–840.
- [50] A.F. Orchard, Magnetochemistry, Oxford University Press, Oxford, 2003.
- [51] G. Pescitelli, S. Lüdeke, A.C. Chamayou, M. Marolt, V. Justus, M. Górecki, L. Arrico, L. Di Bari, M.A. Islam, I. Gruber, M. Enamullah, C. Janiak, Broad-range spectral analysis for chiral metal coordination compounds: (chiro)optical superspectrum of cobalt(II) complexes, *Inorg. Chem.* 57 (2018) 13397–13408.
- [52] A.J. Bridgeman, On the origin of paramagnetism in planar nickel(II) complexes, *Dalton Trans.* (2008) 1989–1992.
- [53] M. Enamullah, M. Al-M. Zaman, M.M. Bindu, M.K. Islam, M.A. Islam, Experimental and theoretical studies of isatin-Schiff bases and their copper(II)-complexes: syntheses, spectroscopy, tautomerism, redox potentials, EPR, PXRD and DFT/TDDFT, *J. Mol. Struct.* 1201 (2020), 127207.
- [54] M. Enamullah, M.A. Quddus, M.M. Rahman, T.E. Burrow, Syntheses and characterization of copper(II)-complexes with N-2-(*R*-pyridyl)salicylaldiminate Schiff base ligands (*R* = H, 4/6-CH₃), *J. Mol. Struct.* 1130 (2017) 765–774.